Electrocatalytic Oxidation and Determination of Hydrazine at an AuCu Nanoparticles – Graphene – Ionic Liquid Composite Film Coated Glassy Carbon Electrode

Lei Shang, *Faqiong Zhao*, *Baizhao Zeng**

The Key Laboratory of Analytical Chemistry for Biology and Medicine (Ministry of Education), College of Chemistry and Molecular Sciences, Wuhan University, Wuhan 430072, P. R. China
tel: +086-27-68752701, fax: 86-27-68754067
*e-mail: bzzeng@whu.edu.cn

Received: April 18, 2012
Accepted: October 10, 2012

Abstract
Gold-copper alloy nanoparticles (AuCu NPs) were electrodeposited on a graphene – ionic liquid composite film (EGN-IL). The AuCu NPs showed high electrocatalysis to the oxidation of hydrazine with a catalytic reaction rate constant of about 5.0×10^4 mol/Ls. In phosphate buffer solutions (pH 6.8) the oxidation current of hydrazine at 0.15 V (vs. SCE) at the resulting electrode (AuCu–EGN-IL/GCE) was linear to its concentration in the range of 0.2–110 μM with a sensitivity of 56.7 μA/mM, and the detection limit was 0.1 μM ($S/N=3$). The electrode was successfully applied to the determination of waste water.

Keywords: AuCu nanoparticle, Graphene, Electrodeposition, Hydrazine, Ionic liquid

DOI: 10.1002/elan.201200209

Supporting information for this article is available on the WWW under http://dx.doi.org/10.1002/elan.201200209.

1 Introduction

Hydrazine is an important compound and can be used as corrosion inhibitor, insecticide, plant-growth regulator and fuel for direct fuel cell systems [1–3]. However, hydrazine is also a carcinogenic, hepatotoxic and mutagenic substance, and can cause blood abnormality and irreversible damage of the nervous system [4–6]. Therefore, the sensitive detection of hydrazine is significant in environment.

So far, several methods have been developed for the determination of hydrazine, including spectrophotometry [7], titrimetry [8], chemiluminescence [9] and ion chromatography [10]. The electrochemical method is rapid and cost-effective, and is also exploited for the detection of hydrazine. For the determination of hydrazine different modified electrodes were prepared in order to lower its overpotential and to enhance the detection sensitivity [11–21]. Among them nano-gold modified electrodes presented good performance and attracted more attention of researchers [16–21]. For example, Yan et al. [16] reported a nanoporous gold (NPG) modified electrode for hydrazine detection, which was prepared by dealloying of AgAu in concentrated nitric acid. Compared with the bulk gold electrode the NPG modified electrode showed enhanced current response and the oxidation potential of hydrazine decreased. Based on the electrodeposition of gold nanoparticles on a choline film coated glassy carbon electrode (GNPs/Ch/GCE), Li et al. [18] developed a sensitive hydrazine sensor. Its response current was 3.4-fold as much as that of a GNPs/GCE.

It is well known, that alloys generally possess many properties superior to their single-metal components [22, 23]. In addition, by incorporating common metals into noble metals the consumption of noble metals can be reduced and more functions may be achieved. Some alloys present good electrocatalysis and have been widely used in the preparation of fuel cells and sensors [24–27]. Such as AuCu alloy, it was used to construct different electrochemical sensors and showed interesting performance [28–30]. Recently, alloys based electrochemical sensors received increasing attention.

Graphene is a novel nanomaterial with many unique characteristics [31, 32], and it has great application potential in electroanalysis field. Generally, the graphene prepared by chemical reduction contains many oxygen-containing groups, which affect its electrocatalytic performance. Recently, the electrochemical preparation of graphene was attempted [33–36], and the resulted graphene showed superior electronic property to that prepared by chemical reduction. In addition, to prevent the aggregation of graphene nanosheets dispersants, such as poly-(diallyldimethyl-ammonium chloride) (PDDA) [37], Nafion [38] and chitosan [39], were often added. Ionic liquids (ILs) could also be used for such purpose [40,1]. Recently, graphene was used to fabricate hydrazine sensor and it

improved the current response [42–44]. However, to the best of our knowledge there are no reports on the voltammetric determination of hydrazine by using alloy nanoparticle or alloy nanoparticle – graphene hybrid film modified electrodes. Nevertheless, when alloy nanoparticles and graphene are used to fabricate electrochemical sensors they may produce synergic interaction and the performance of sensors may be further improved.

In this paper, an IL (i.e. 1-(2-hydroxyethyl)-3-methylimidazolium bis(trifluoromethanesulfonyl)imide) – graphene composite film is prepared by electrochemical reduction, and then AuCu nanoparticles are electrodeposited on it. The structure and electrochemical property of the resulting alloy nanoparticle – graphene – IL hybrid film are studied by scanning electron microscopy (SEM), energy dispersive X-ray spectroscopy (EDX), X-ray photoelectron spectroscopy (XPS), X-ray diffraction (XRD) and voltammetry. The hybrid film exhibits high catalytic activity for the electrochemical oxidation of hydrazine, and thus it is used for hydrazine sensing.

2 Experimental

2.1 Reagents

$HAuCl_4$ and $CuSO_4$ were purchased from Sinopharm Chemical Reagent Co. Ltd. (Shanghai, China). The ionic liquid 1-(2-hydroxyethyl)-3-methylimidazolium bis(trifluoromethanesulfonyl)imide (purity: 99%) was provided by Lanzhou Institute of Chemical Physics (Lanzhou, China) and was used as received. Graphene oxide (GO) came from Xianfeng Reagent Co. Ltd. (Nanjing, China). Hydrazine was the product of Sinopharm Chemical Reagent Co. Ltd. (Shanghai, China), and 20 mM hydrazine stock solutions were prepared with water and stored in a refrigerator. The working solutions were prepared by diluting the stock solution with phosphate buffer solution (PBS: pH 6.8). All other chemicals used were of analytical reagent grade. The water used was redistilled.

2.2 Apparatus

Electrodeposition, cyclic voltammetric (CV) and chronoamperometric experiments were performed on a CHI 440 electrochemical workstation (CH Instrument Company, Shanghai, China). The electrochemical impedance spectroscopy was recorded with a CHI 660D electrochemical workstation (CH Instrument Company, Shanghai, China). A conventional three-electrode system was adopted. The working electrode was a modified glassy carbon electrode (diameter: 2 mm) or a glass substrate (10 mm × 10 mm × 2.2 mm) coated with an indium tin oxide (ITO), and the auxiliary electrode and reference electrode were a platinum wire and a saturated calomel electrode (SCE), respectively. The SEM images and energy dispersive X-ray spectroscopy were obtained by using a Hitachi X-650 SEM (Hitachi Co., Japan). X-ray diffraction data were recorded with a Bruke D8 diffractometer (Germany) using Cu Kα radiation (40 kV, 40 mA) with a Ni filter. X-ray photoelectron spectroscopy was performed on an Escalab MKII spectrometer (VG Co., UK), using Mg KR radiation (1253.6 eV) at a pressure of 2.0×10^{-10} mbar. The peak positions were internally referenced to the C 1s peak at 284.6 eV. All measurements were conducted at room temperature.

2.3 Preparation of Modified Electrodes

GO was dispersed in redistilled water to prepare a 1 mg/mL GO suspension. Then 0.5 mL GO suspension was mixed with 0.5 mL IL solution (2.5 μL/mL, in *N*,*N*-dimethylformamide), with the aid of ultrasonication. Then, 4 μL of the resulted suspension was transferred on a cleaned GCE and the solvent was evaporated in air, thus a GO-IL film coated electrode (GO-IL/GCE) was obtained. The GO-IL/GCE was immersed in a 0.2 M Na_2SO_4 aqueous solution and the potential was hold at −1.3 V (vs. SCE) for 600 s [45]. Thus GO was reduced to graphene and the obtained electrode was denoted as EGN-IL/GCE. Then AuCu nanoparticles were electrodeposited on the surface of EGN-IL/GCE. The deposition potential was −0.4 V, the deposition time was 400 s and the electrolyte solution was a 0.2 M Na_2SO_4 aqueous solution containing 0.5 mM $HAuCl_4$ and 0.5 mM $CuSO_4$. The obtained AuCu [1:1, i.e., the ratio of $c(HAuCl_4)$/$c(CuSO_4)$] –EGN-IL/GCE (or ITO) was washed carefully with redistilled water and then dried at room temperature. For comparison AuCu/GCE, Au–EGN-IL/GCE and Cu–EGN-IL/GCE were fabricated through the similar method. Before measurement, the working electrode was conditioned by repeating potential scan between −0.2 V and 0.6 V in a PBS until a stable CV curve was obtained.

3 Results and Discussion

3.1 Morphological Analysis

As shown in Figure 1, the EGN-IL composite film is quite uniform, probably due to the binding and blanketing effect of viscous IL. After AuCu is electrodeposited on it, many small particles (diameter: about 50 nm) occur. They are smaller than those electrodeposited on ITO, and the particle density is much higher than that on ITO. This is because the EGN can provide many sites for the formation of AuCu nucleus and IL can enhance the nucleation rate due to its low interface tension [25]. As more AuCu nucleuses form on the EGN-IL composite film the resulting AuCu particles become smaller. In addition, the IL can also form a hydrophobic area outside the AuCu particles and acts as a stabilizer, which can avoid the aggregation of AuCu particles to some extent. Therefore, the EGN-IL is a better support for the electrodeposition of AuCu nanoparticles. It should be pointed out, when the IL is replaced by 1-butyl-3-methylimidazolium hexafluorophosphate and 1-octyl-3-methylimidazoli-

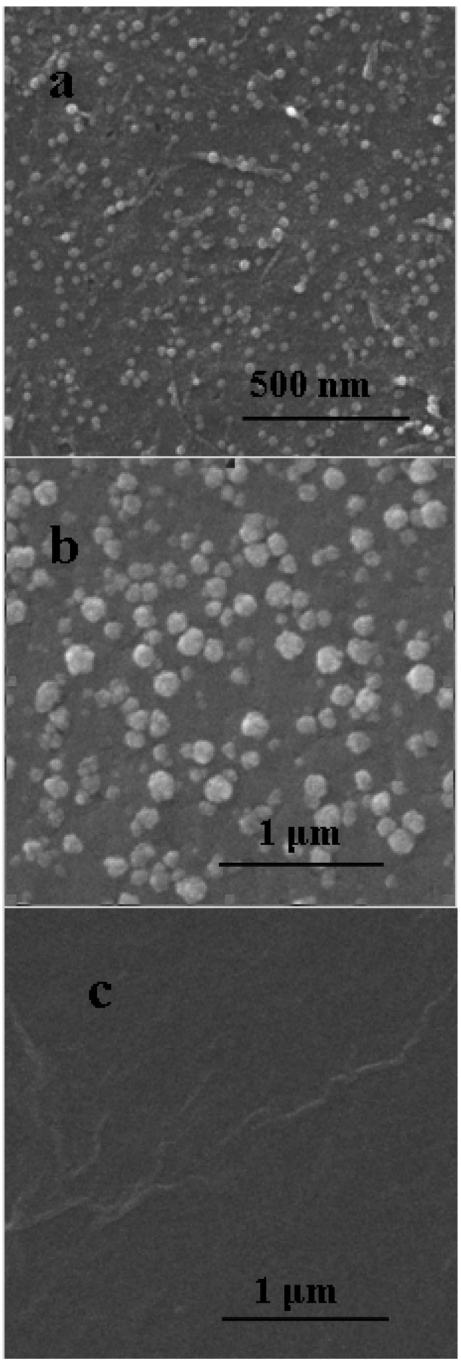

Fig. 1. SEM images of AuCu-EGN-IL/ITO (a), AuCu/ITO (b) and EGN-IL/ITO (c). The solution for electrodeposition: 0.2 M Na_2SO_4 containing 0.5 mM $HAuCl_4$ and 0.5 mM $CuSO_4$; electrodeposition potential: −0.4 V; electrodeposition time: 400 s.

um hexafluorophosphate GO cannot be well dispersed and the resulting GO-IL film is not so uniform.

3.2 Structure and Composition Analysis

The composition of AuCu particles is determined by EDX (see Supporting Information, Figure S1), and the atom ratio of Au/Cu is about 61 : 39, which is higher than the ratio of $c(HAuCl_4)/c(CuSO_4)$ in the electrolyte solution. This means that the electrodeposition of Au is easier than that of Cu under this condition. We think it is related to the different diffusion rate of $AuCl_4^-$ and Cu^{2+}, the different stability of Au and Cu, their competition for deposition sites and the alloy structure.

Figure 2A shows the XRD patterns of Au (c) and AuCu (d) particles electrodeposited on EGN-IL/ITO. The diffraction patterns display a series of broad Bragg peaks, which are typical for material of limited structural coherence. The peaks around 38.18°, 44.38°, 64.67°, 77.71° and 81.86° can be assigned to Au (111), (200), (220), (311) and (222), respectively. They are in line with the standard XRD pattern of Au (b) (JCPDS 04-0784). The peaks around 50° and 60° are produced by ITO. Compared with the corresponding peaks of Au the peaks of AuCu (d) shift to higher 2θ values and fall well between the peaks of pure Au (b) and pure Cu (a, JCPDS 04-0836), indicating that the AuCu nanoparticles are alloy rather than a mixture of monometallic nanoparticles.

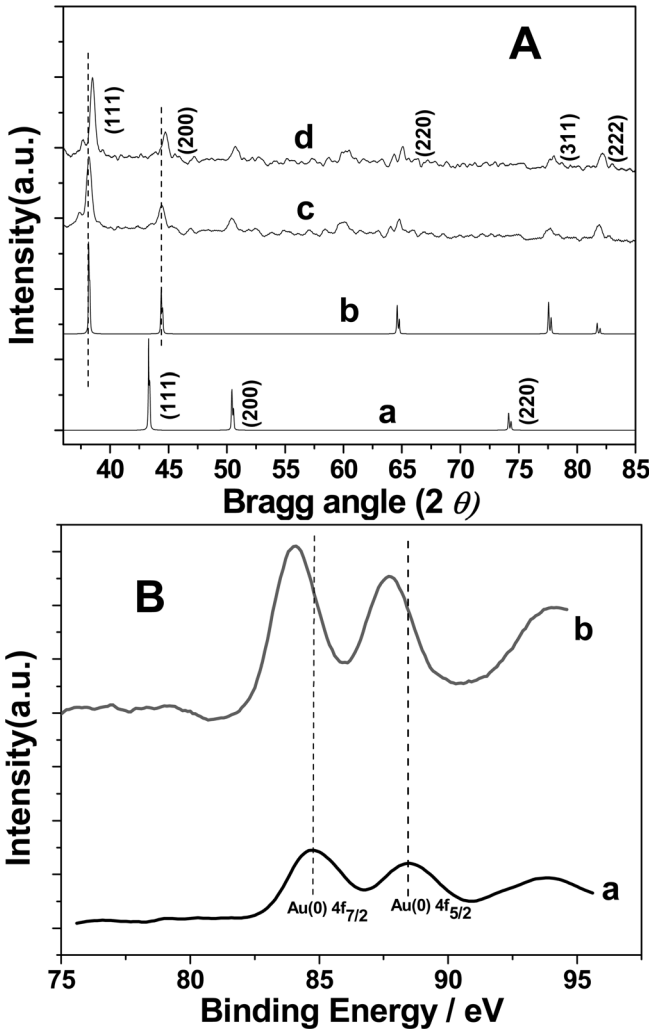

Fig. 2. (A) Standard XRD patterns of Cu (a) and Au (b); XRD patterns of Au (c) and AuCu particles (d) electrodeposited on EGN-IL film. (B) XPS spectra of Au 4f for Au–EGN-IL/GCE (a) and AuCu–EGN-IL/GCE (b).

XPS spectra of Au and AuCu nanoparticles are shown in Figure 2B. The peaks at 84.71 eV and 88.44 eV can be assigned to the Au $4f_{7/2}$ binding energy and Au $4f_{5/2}$ binding energy, respectively. For AuCu (b) the Au 4f binding energy decreases, indicating that the electronic structure of Au is altered in the AuCu (so-called electronic effect) and Au and Cu form alloy. This is in agreement with the result of XRD experiment.

3.3 Electrocatalytic Oxidation of Hydrazine

The CVs of the bare GCE (curves a and b), EGN-IL/GCE (curves c and d), Au-EGN-IL/GCE (curves e and f) and AuCu–EGN-IL/GCE (curves g and h) in different solutions are presented in Figure 3A. Hydrazine does not produce any peaks at the bare GCE. When the GCE is replaced by the EGN-IL/GCE, hydrazine exhibits an oxidation peak at about 0.3 V, which can be attributed to the promotion of EGN-IL to the electron transfer of hydrazine. However, the peak is broad and the peak current is small. When Au nanoparticles were electrodeposited on the EGN-IL film the oxidation potential of hydrazine decreases and the peak current increases. This should be attributed to the enhanced surface area and electron-transfer rate by Au nanoparticles. For AuCu–EGN-IL/GCE, the peak current of hydrazine is greater, meaning that the AuCu–EGN-IL/GCE has higher catalytic activity to the oxidation of hydrazine. As the peak potential is almost the same as that of Cu peak, we think that the catalysis of AuCu nanoparticles to hydrazine oxidation is associated with the oxidation of Cu in the alloy (e.g. $AuCu^0 \rightarrow AuCu^{2+} + 2e$). The oxidized Cu then interacts with hydrazine.

Figure 3B shows the CVs of hydrazine at AuCu/GCE and AuCu–EGN-IL/GCE. It is clear that hydrazine produces a much higher peak at the AuCu–EGN-IL/GCE than at the AuCu/GCE. The reason is that more AuCu nanoparticles are electrodeposited on the EGN-IL/GCE. For comparison, Pt, Pd, Ru, Ni and Co are also tested, but they show poor catalysis in this case.

Figure 3C displays the impedance spectroscopy of bare GCE, EGN-IL/GCE and AuCu–EGN-IL/GCE. As hydrazine shows large overpotential at GCE, the electron transfer resistance (R_{ct}) of bare GCE (Figure 3C, Inset) is quite great, which is much greater than that of EGN-IL/GCE and AuCu-EGN-IL/GCE. In comparison with the EGN-IL/GCE (curve b), the AuCu–EGN-IL/GCE exhibits smaller electron transfer resistance (curve a), indicating that the AuCu–EGN-IL/GCE has higher conductivity and the electron transfer of hydrazine occurs more easily at it.

As the ratio of $c(HAuCl_4)/c(CuSO_4)$ affects the composition and the amount of alloy particle electrodeposited, the current response of hydrazine at the resulting AuCu–EGN-IL/GCE is also dependent on it (see Supporting Information, Figure S2). Experimental result shows that the peak current of hydrazine gradually increases with the ratio of $c(HAuCl_4)/c(CuSO_4)$ changing from 10:0 to 1:1.

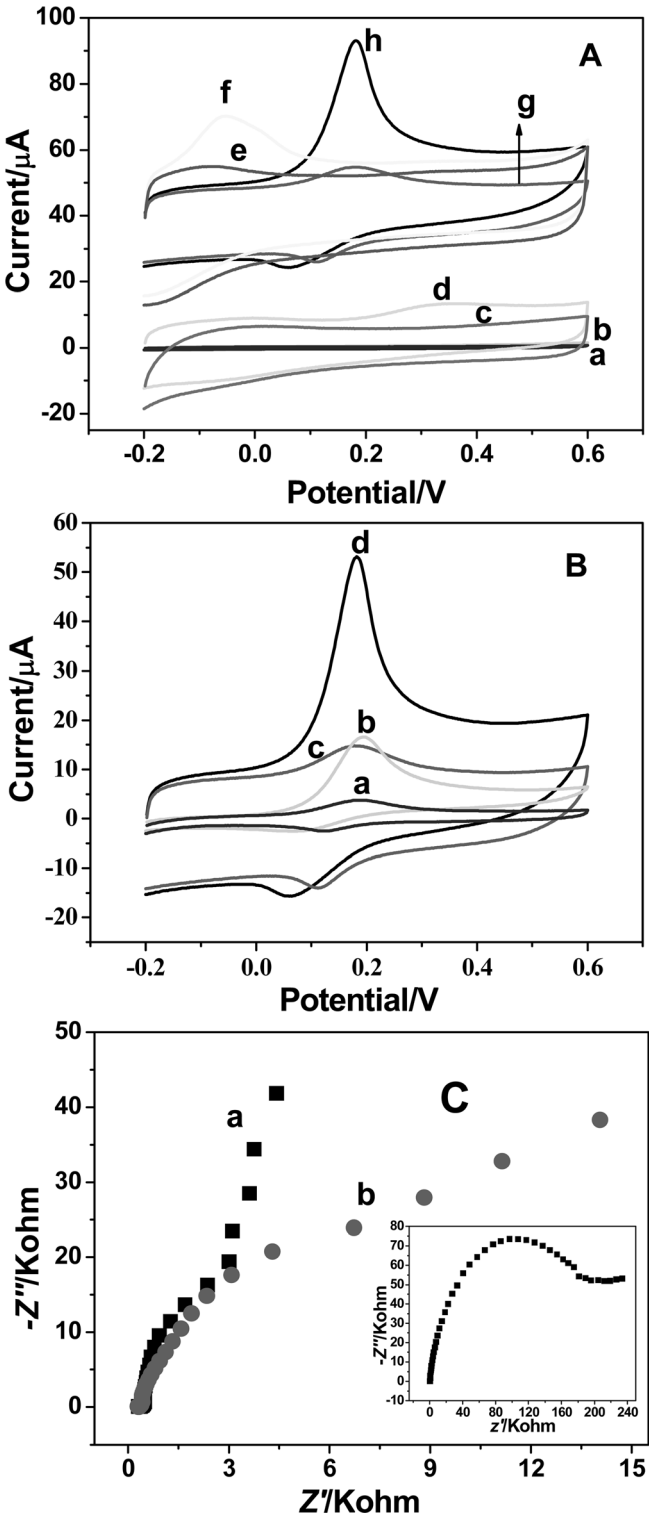

Fig. 3. (A) CVs of bare GCE (a, b), EGN-IL/GCE (c, d), Au–EGN-IL/GCE (e, f) and AuCu–EGN-IL/GCE (g, h) in 0.1 M PBS (pH 6.8) containing 0 (a, c, e, g) and 3.0×10^{-4} M (b, d, f, h) hydrazine. In order to distinguish them several curves (e, f, g, h are moved along the ordinate axis to some extent. (B) CVs of AuCu/GCE (a, b) and AuCu–EGN-IL/GCE (c, d) in 0.1 M PBS (pH 6.8) containing 0 (a, c) or 3.0×10^{-4} M (b, d) hydrazine. Scan rate: 100 mV/s. (C) Nyquist plots of AuCu–EGN-IL/GCE (a), EGN-IL/GCE (b) and bare GCE (c) in 0.1 M PBS (pH 6.8) containing 3.0×10^{-4} M hydrazine.

However, when the ratio is further decreased, the peak current declines. Therefore, the concentrations of $HAuCl_4$ and $CuSO_4$ are kept the same in the following experiments. The Cu–EGN-IL/GCE hardly shows stable electrocatalysis to the oxidation of hydrazine under this condition. But when Cu and Au form alloy the obtained AuCu–EGN-IL/GCE is stable enough. This means that Au and Cu can coordinate in catalyzing the oxidation of hydrazine.

Solution pH is another important factor influencing the electrochemical response of hydrazine. Although the peak current of hydrazine is larger at pH 6.4 (see Supporting Information, Figure S3), pH 6.8 is selected in this experiment as the AuCu–EGN-IL/GCE electrode is more stable at this pH. With pH changing the peak potential (E_p) shifts and the slope of E_p vs. pH plot is about −78 mV/pH. This suggests that the electrochemical process should involve proton-transfer. It is similar to that reported in literature [46].

In addition, the influence of the scan rate (v) is investigated (see Supporting Information, Figure S4). As a result, in the range studied (30–300 mV/s) the peak current and $v^{1/2}$ show the linear relationship i_p (μA) = $-9.45+2.38\ v^{1/2}$ (v: mV/s, $R=0.991$). This indicates that the electrochemical process is diffusion-controlled.

3.4 Estimation of Diffusion Coefficient and Catalytic Reaction Rate Constant

Figure 4 presents the chronoamperometric curves of AuCu–EGN-IL/GCE in hydrazine solutions. As can be seen, the oxidation current of hydrazine quickly decreases in initial several seconds and then gradually reaches a stable value. The current (I) vs. $t^{-1/2}$ plots are worked out and they present linear relationship in certain range. The relationship between the slope (S) of the linear segment and the hydrazine concentration can be expressed as S (mA $s^{-1/2}$) = 1.40 + 0.023c (μM). According to the slope and Cottrell's law (i.e. $I = nFA\ C\ D^{1/2}\ \pi^{-1/2}\ t^{-1/2}$, the symbols have normal meaning) [47], the diffusion coefficient of hydrazine can be estimated and it is about 1.2×10^{-5} $cm^2\ s^{-1}$.

When the time is more than 5.0 ms, the catalytic reaction rate constant (k) can be estimated on the basis of the equation [48]: $I_c/I_L=\pi^{1/2}(kc_0t)^{1/2}$, where I_c is the catalytic current in the presence of hydrazine, I_L is the limiting diffusion current in the absence of hydrazine, c_0 is the bulk concentration and t is the time. The chronoamperometric response curves of AuCu–EGN-IL/GCE are shown in Figure 4B for solutions containing 0 and 40 μM hydrazine. According to the slope of $I_c/I_L-(c_0t)^{1/2}$ plot, k is estimated to be 5.0×10^4 mol/L s.

3.5 Amperometric Measurement of Hydrazine

Under the optimized conditions, the chronoamperometric curve of hydrazine is recorded (Figure 5). The response current is linear to hydrazine concentration in the range

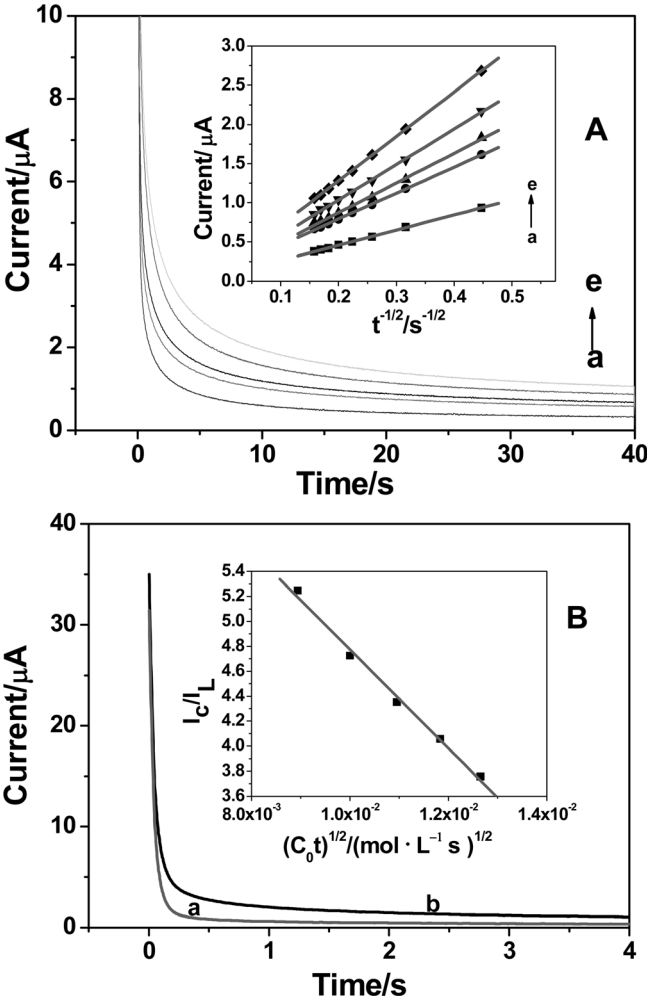

Fig. 4. (A) Chronoamperometric response curves of AuCu–EGN-IL/GCE in PBS (0.1 M, pH 6.8) containing 40 μM (a), 80 μM (b), 100 μM (c), 140 μM (d) and 180 μM (e) hydrazine. Applied potential: 0.15 V; Inset: Corresponding current I vs. $t^{-1/2}$ plots. (B) Chronoamperometric response curves of AuCu–EGN-IL/GCE in PBS containing 0 μM (a) or 40 μM (b) hydrazine. Inset: Relationship between I_c/I_L and $(c_0t)^{1/2}$.

of 0.2 μM–0.11 mM, with a sensitivity of 56.7 μA/mM. The detection limit is estimated to be 0.1 μM ($S/N=3$). The AuCu–EGN-IL/GCE exhibits low detection limit and high sensitivity for hydrazine in comparison with other modified electrodes (Table 1).

3.6 Stability, Reproducibility and Interference of Foreign Species

To test the reproducibility and stability of the modified electrode, 40 μM hydrazine was detected with seven electrodes prepared in the same way, and the relative standard deviation (*RSD*) of the peak current was 9.5%, indicating that the modified electrode had acceptable reproducibility. Twelve successive measurements yielded an *RSD* of 5.6% by using one electrode, indicating that the electrode could be used for the repeated detection of hydrazine. The storage stability of the modified electrode

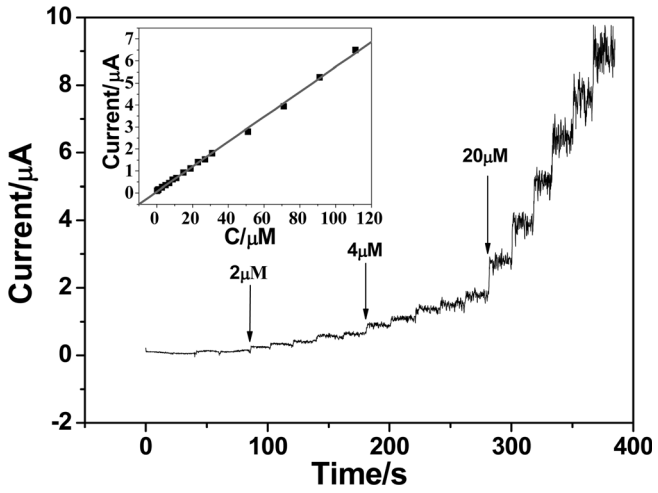

Fig. 5. The amperometric response of AuCu–IL-GN/GCE to hydrazine in 0.1 M PBS. Solution pH: 6.8; applied potential: 0.15 V. Inset: Calibration curve of response current versus hydrazine concentration.

Table 1. Comparison of different modified electrodes for hydrazine determination.

Electrode	Detection limit (μM)	Linear range (μM)	Reference
ZnO nanonails	0.2	0.1–1.2	[14]
MnO_2-graphene oxide	0.16	3–1120	[15]
Nano Au-thiol-ssDNA	0.56	100–10^5	[17]
Au-choline	0.1	0.5–5000	[18]
Au-ZnO-MWNT	0.15	0.5–1800	[20]
PSS-graphene	1	3–300	[43]
PB-graphene	7	10–3000	[44]
AuCu-EGN-IL	0.1	0.2–110	This work

was also examined. After one-week store at 4 °C in a refrigerator, the response current retained 87 % of its initial value. After one month it became 71 %.

The interference of some foreign species for the determination of hydrazine was tested. The tolerance limit was defined as the maximum concentration of the foreign species that causes a relative error of 5 % for the determination of 20 μM hydrazine. The results showed that 250-fold of glucose, sucrose, ethanol, Cl^-, Br^-, NH_4^+, and Mg^{2+}, and 500-fold of NO_3^- did not interfere with the determination of hydrazine. The better selectivity of the AuCu–EGN-IL/GCE is related to the low applied potential and the interaction between hydrazine and AuCu nanoparticles, in addition to the block effect of IL to some species.

3.7 Application

In order to evaluate the practical feasibility of the proposed method for the determination of hydrazine, waste water samples were determined. For the determination 1 mL waste water was diluted to 10 mL with 0.1 M PBS (pH 6.8). But no hydrazine was detected in the samples. Standard hydrazine solutions were added to the samples to estimate the recovery. The data are shown in Table 2 and the recovery is acceptable.

Table 2. Recovery of standard solutions added in water samples.

Sample	Added (μM)	Found (μM)	Recovery (%)
Petrochemical waste water	0	–	–
	4	3.9	97.5
	8	7.9	98.8
	28	28.5	101.2
	48	48.4	100.8
Dye waste water	0	–	–
	4	4.1	102.5
	8	7.8	97.5
	48	46.6	97.1
	88	87.3	99.2

4 Conclusions

An EGN-IL film can be fabricated on a GCE by electrochemical reduction and AuCu nanoparticles can be electrodeposited on it. The resulted modified electrode (AuCu–EGN-IL/GCE) exhibits strong electrocatalytic activity to the oxidation of hydrazine. The oxidation potential of hydrazine decreases to 0.15 V, the peak current increases and the detection limit decreases. The AuCu–EGN-IL/GCE is suitable for the amperometric determination of hydrazine. This work paves a new way for constructing sensitive sensors.

Acknowledgements

The Authors appreciate the financial support of the *National Natural Science Foundation of China* (Grant No.: 21075092), the *State Key Laboratory of Advanced Technology for Materials Synthesis and Processing* (*Wuhan University of Technology*, Grant No. 2010-KF-12), and the *State Key Laboratory of Electroanalytical Chemistry*, *Changchun Institute of Applied Chemistry, China*.

References

[1] W. X. Yin, Z. P. Li, J. K. Zhu, H. Y. Qin, *J. Power Sources* **2008**, *182*, 520.
[2] K. Yamada, K. Yasuda, N. Fujiwara, Z. Siroma, H. Tanaka, Y. Miyazaki, T. Kobayashi, *Electrochem. Commun.* **2003**, *5*, 892.
[3] S. Amlathe, V. K. Gupta, *Analyst* **1988**, *113*, 1481.
[4] S. Garrod, M. E. Bollard, A. W. Nicholls, S. C. Connor, J. Connelly, J. K. Nicholson, E. Holmes, *Chem. Res. Toxicol.* **2005**, *18*, 115.
[5] S. M. Golabi, H. R. Zare, *J. Electroanal. Chem.* **1999**, *465*, 168.

[6] A. Poso, A. V. Wright, J. Gynther, *Mutat. Res.* **1995**, *332*, 63.
[7] A. Safavi, F. Abbasitabar, M. R. H. Nezhad, *Chem. Anal.* **2007**, *52*, 835.
[8] J. S. Budkuley, *Mikrochim. Acta* **1992**, *108*, 103.
[9] A. Safavi, M. A. Karimi, *Talanta* **2002**, *58*, 785.
[10] R. Gilbert, R. Rioux, S. E. Saheb, *Anal. Chem.* **1984**, *56*, 106.
[11] L. Zheng, J. F. Song, *Talanta* **2009**, *79*, 319.
[12] M. A. Kamyabi, O. Narimani, H. H. Monfared, *J. Electroanal. Chem.* **2010**, *644*, 67.
[13] C. Batchelor-McAuley, C. E. Banks, A. O. Simm, T. G. J. Jones, R. G. Compton, *Analyst* **2006**, *131*, 106.
[14] A. Umar, M. M. Rahman, S. H. Kim, Y. B. Hahn, *Chem. Commun.* **2008**, 166.
[15] J. Y. Lei, X. F. Lu, W. Wang, X. J. Bian, Y. P. Xue, C. Wang, L. J. Li, *RSC Adv.* **2012**, *2*, 2541.
[16] X. L. Yan, F. H. Meng, S. Z. Cui, J. G. Liu, J. Gu, Z. G. Zou, *J. Electroanal. Chem.* **2011**, *661*, 44.
[17] G. H. Chang, Y. L. Luo, W. B. Lu, J. M. Hu, F. Liao, X. P. Sun, *Thin Solid Films* **2011**, *519*, 6130.
[18] J. Li, H. Q. Xie, L. F. Chen, *Sens. Actuators B* **2011**, *153*, 239.
[19] Q. F. Yi, W. Q. Yu, *J. Electroanal. Chem.* **2009**, *633*, 159.
[20] C. H. Zhang, G. F. Wang, Y. L. Ji, M. Liu, Y. H. Feng, Z. D. Zhang, B. Fang, *Sens. Actuators B* **2010**, *150*, 247.
[21] B. K. Jena, C. R. Raj, *J. Phys. Chem. C* **2007**, *17*, 6228.
[22] F. U. Renner, A. Stierle, H. Dosch, D. M. Kolb, T. L. Lee, J. Zegenhagen, *Nature* **2006**, *439*, 707.
[23] J. A. Rodriquez, D. W. Goodman, *Science* **1993**, *260*, 1527.
[24] F. Xiao, F. Q. Zhao, L. Z. Deng, B. Z. Zeng, *Electrochem. Commun.* **2010**, *12*, 620.
[25] Y. F. Zhang, G. P. Guo, F. Q. Zhao, Z. R. Mo, F. Xiao, B. Z. Zeng, *Electroanalysis* **2010**, *22*, 223.
[26] F. Q. Zhao, F. Xiao, B. Z. Zeng, *Electrochem. Commun.* **2010**, *12*, 168.
[27] F. Xiao, F. Q. Zhao, D. P. Mei, Z. R. Mo, B. Z. Zeng, *Biosens. Bioelectron.* **2009**, *24*, 3481.
[28] C. Y. Tai, J. L. Chang, J. F. Lee, T. S. Chan, J. M. Zen, *Electrochim. Acta* **2011**, *56*, 3115.
[29] D. Y. Liu, Q. M. Luo, F. Q. Zhou, *Synth. Met.* **2010**, *160*, 1745.
[30] M. Tominaga, Y. Taema, I. Taniguchi, *J. Electroanal. Chem.* **2008**, *624*, 1.
[31] A. Peigney, C. Laurent, E. Flahaut, R. R. Bacsa, A. Rousset, *Carbon* **2001**, *39*, 507.
[32] A. K. Geim, K. S. Novoselov, *Nat. Mater.* **2007**, *6*, 183.
[33] H. L. Guo, X. F. Wang, Q. Y. Qian, F. B. Wang, X. H. Xia, *ACS Nano* **2009**, *3*, 2653.
[34] Y. Y. Shao, J. Wang, M. Engelhard, C. M. Wang, Y. M. Lin, *J. Mater. Chem.* **2010**, *20*, 743.
[35] M. Zhou, Y. L. Wang, Y. M. Zhai, J. F. Zhai, W. Ren, F. Wang, S. J. Dong, *Chem. Eur. J.* **2009**, *15*, 6116.
[36] S. Wu, X. Q. Lan, L. J. Cui, L. H. Zhang, S. Y. Tao, H. N. Wang, M. Han, Z. G. Liu, C. G. Meng, *Anal. Chim. Acta* **2011**, *699*, 170.
[37] J. D. Qiu, G. C. Wang, R. P. Liang, X. H. Xia, H. W. Yu, *J. Phys. Chem. C* **2011**, *115*, 15639.
[38] B. G. Choi, H. Park, T. J. Park, M. H. Yang, J. S. Kim, S. Y. Jang, N. S. Heo, S. Y. Lee, J. Kong, W. H. Hong, *ACS Nano* **2010**, *4*, 2910.
[39] Q. Zeng, J. S. Cheng, X. F. Liu, H. T. Bai, J. H. Jiang, *Biosens. Bioelectron.* **2011**, *26*, 3456.
[40] Z. M. Liu, Z. L. Wang, Y. Y. Cao, Y. F. Jing, Y. L. Liu, *Sens. Actuators B* **2011**, *157*, 540.
[41] M. H. Yang, B. G. Choi, H. Park, T. J. Park, W. H. Hong, S. Y. Lee, *Electroanalysis* **2011**, *23*, 850.
[42] Y. Wang, Y. Wan, D. Zhang, *Electrochem. Commun.* **2010**, *12*, 187.
[43] C. Wang, L. Zhang, Z. H. Guo, J. G. Xu, H. Y. Wang, K. F. Zhai, X. Zhuo, *Microchim. Acta* **2010**, *169*, 1.
[44] Y. Y. Jiang, X. D. Zhang, C. S. Shan, S. C. Hua, Q. X. Zhang, X. X. Bai, L. Dan, L. Niu, *Talanta* **2011**, *85*, 76.
[45] M. Du, T. Yang, K. Jiao, *J. Mater. Chem.* **2010**, *26*, 9253.
[46] W. M. Costa, A. L. B. Marques, E. P. Marques, C. W. B. Bezerra, E. R. Sousa, W. S. Cardoso, C. J. Song, J. J. Zhang, *J. Appl. Electrochem.* **2010**, *40*, 375.
[47] A. J. Bard, L. R. Faulkner, *Electrochemical Methods: Fundamentals and Applications*, Wiley, New York, **1980**.
[48] Z. Galus, *Fundamentals of Electrochemical Analysis*, Ellis Horwood, New York, **1994**.

